Journal of Physics and Chemistry of Solids 199 (2025) 112537

Contents lists available at ScienceDirect

Journal of Physics and Chemistry of Solids

journal homepage: www.elsevier.com/locate/jpcs

Adsorption of CO and CO_2 interaction with (7,0) AlN nanotubes to enhance sensing capabilities: A DFT approach

Nafiu Suleiman [a], Vitus Apalangya [b], Kwabena Kan-Dapaah [c], Bismark Mensah [a], Van W. Elloh [d], Abu Yaya [a], Eric K.K. Abavare [e,*]

[a] Department of Materials Science and Engineering, University of Ghana, CBAS, Ghana
[b] Department of Food Process Engineering, University of Ghana, CBAS, Ghana
[c] Department of Biomedical Engineering, University of Ghana, CBAS, Ghana
[d] Department of Biomedical Engineering, Koforidua Technical University, Koforidua, Ghana
[e] Department of Physics, Kwame Nkrumah University of Science and Technology, Kumasi, Ghana

ARTICLE INFO

Keywords:
AlNNT
Si-AlNNT
CO
CO_2
Density functional theory (DFT)
Nanotubes
HOMO–LUMO
Sensors

ABSTRACT

We performed atomic and electronic structure calculations to examine the adsorption of carbon dioxide (CO_2) and carbon monoxide (CO) gases on single-wall (7,0) aluminum nitrides nanotubes (AlNNTs) as gas sensor nanomaterials. We employed local density approximation (LDA) in the frame of density functional theory to elucidate the sensory parameters such as adsorption energy, detection sensitivity and recovery times to evaluate the molecular interactions on the metal oxide surface and their potential applications for gas sensing. The findings suggest that CO_2 showed strong adsorption on pristine (7,0) AlNNTs with an adsorption energy of ~ – 23.58 kcal/mol. Although a detection capacity of 96.6 % could be achieved, its recovery time was protracted to about 1.35 days, limiting its ability for rapid sensing material. However, silicon-doped (7,0) AlNNTs displayed moderate CO_2 adsorption energy of – 17.56 kcal/mol with sensing potential of 80.2 % and fast recovery time in less than 5.13 s. CO adsorption on pristine (7,0) showed strong interaction but with poor detection and recovery times. Nevertheless, the Si-doped (7,0) showed adsorption energy of ~ – 18.67 kcal/mol and high sensing capacity of about 80.4 % with relatively fast recovery times of approximately 32.64 s, making it promising candidate for CO detector material compared with the pristine nanotubes. In all calculations, the basis set superposition error correction factor (BSSE) gave low values for the adsorption energies.

1. Introduction

Some gases like air are critical to human life and environmental situations, just as CO and CO_2 have economic importance to plants in our environment and human health. One unique characteristics property of CO is that, it is colorless and odorless gas produced by the incomplete combustion of different carbonaceous substances including fuels, gases, wood and others [1,2], partially emitted by exhausts fumes from motor vehicles, power plants, wildfires and incinerator waste plants, but also produced atmospherically by photoreactions on methane, non-methane hydrocarbons and other volatile organic compounds of the air, and in reactions with surface waters and soil [2]. In toxic doses, this gas, emitted as a by-product of combustion of fossil fuels, causes headaches, vomiting and dizziness, and can be fatal [1–3].

Carbon dioxide emissions caused by human activities such as fossil fuel combustion increases the heat trap in the Earth's surroundings (global warming), and leads to housing and transportation issues [1–5]. High levels of carbon monoxide, according to the World Health Organization (WHO), may lead to coma or death. In the United States, almost 400 people die per year by carbon monoxide poisoning not including those that come from fires according to the Environmental Protection Agency (EPA) [6–11]. This same challenge associated with CO are similar with CO_2 gas as well. According to the Intergovernmental Panel on Climate Change (IPCC), human-induced activities such as fossil fuel combustion are responsible for the observed climate change and CO_2 emissions increase as one of the causative agents [12–18].

Prior to the beginning of the 20th century, the atmospheric concentration of CO_2 stood at 280 parts per million (ppm), and now exceeds 400 ppm [16,19–23]. As a result, the Earth is getting warmer with an unusual extreme weather events more frequent [24–32] in recent times.

* Corresponding author.
E-mail address: eabavare@yahoo.com (E.K.K. Abavare).

https://doi.org/10.1016/j.jpcs.2024.112537
Received 4 November 2024; Received in revised form 5 December 2024; Accepted 25 December 2024
Available online 26 December 2024

In addition to their monumental effects on both human and environmental circumstances, CO and CO_2 are catalogues of considerable economic significance. The costs of addressing health effects of air pollution and adapting to climate change are projected to rise [33–38].

The search for new materials for detection of CO and CO_2 is crucial as a consequence a newly emerged class of nanomaterials has entered the arena due to their ubiquitous unique properties is the so-called aluminum nitride nanotubes (AlNNTs). This exceptional nanomaterial has shown to be highly resistant to heat, mechanically robust, chemically inert, with high thermal conductivity, which makes it a material of choice for thermal regulation systems, construction, composites, sensors, energy conservation apparatus, and other uses [39]. The AlNNT surface could be created using chemical vapour deposition, chemical etching and electrochemical synthesis techniques [39–44]. Recently, this new emergent material is rapidly developing at high speed, with numerous studies on fabrication, characterization and applications. Research studies are still ongoing to fully understand the fundamental properties and behavior of AlNNTs, as well as to unveil potential applications in industry. The breaking through advances in this subject show encouraging new results which may lay the ground for the feasibility of AlNNTs as versatile and high-performance nanomaterials for device application [43–46].

In recent studies, the adsorption behavior of O_2 molecules on silicon-doped graphene ($C_{53}H_{18}Si$) has been explored. Kuzmin and Shainyan (2020) discovered that the adsorption of O_2 on silicon proceeded without any barriers, resulting in the formation of exclusively atop intermediate. The adsorption energy for this process was found to be −2.40 eV. Interestingly, the barrier to dissociation of O_2 adsorbed on Si-doped graphene was approximately 16 times lower compared to pristine graphene [47].

In a separate investigation, Zhao et al. (2012) focused on graphene doped with a single Si atom, achieved by replacing one carbon atom with a silicon atom. The adsorption process was studied specifically for the doped site. Notably, the only observed adsorption occurred between the oxygen atom of the H_2O molecule and the silicon atom. It should be noted that the H_2O molecule did not adsorb onto the silicon atom from its hydrogen atoms or other adjacent positions [48]. Additionally, Milad et al. (2020) reported an adsorption energy of −29.92 kcal/mol, which is approximately −1.297 eV, for the interaction between H_2O molecules and Si-doped graphene. This finding aligns with the previous study conducted by Zhao et al. (2012) [49]. Overall, these findings contribute to the understanding of adsorption processes and pave the way for the development of more efficient catalysts and sensors, particularly in the context of CO and CO_2 sensing in the air.

AlNNTs nanotubes that are doped with other chemical elements also offers another interesting subclass of nanomaterials due to modification of their electronic properties. These AlNNTs have unique characteristics and are expected to find future device applications, especially in sensing [49–54]. Doped AlNNTs (Cu, C and Ti) have been found to enhance significantly the detection of certain gases, for example, HCOH and NH_3 [52,54]. Impurities modifications can similarly influence the electronic properties and tune the bandgap of AlNNTs that make them suitable for gas detection applications. For instance, doping Cu into AlNNTs changes the nanotube properties from n-type to p-type semiconductor, hence enhancing its detection ability. These changes enhance the detection sensitivity and specificity of certain chemicals [51,55].

Making AlNNTs impure brings along many advantages for sensing applications. Foremost, the electrical properties of AlNNTs are going to change by doping impurities. The conductivity and the bandgap of AlNNTs would ensure that the sensory material could have special interaction with the targeted matter. It is believed that by choosing a suitable dopant and controlling its composition and quantity, these sensing nanomaterials could be fine-tuned to detect a particular chemical entity [51]. Similarly, impurities generate energy bandgap imperfections in AlNNTs, and these grow active reaction positions for chemical responses. As a result, this may cause an intense absorption and obvious receptive response to deal with matter than without impurities. These facilitates AlNNTs dopants absorbing and responding to specific chemicals accurately and sensitively due to their impurity generated imperfections in energy bandgap region [49–54]. It should be noted that the dopant type is determined by the nature of the adsorbing molecules. In view of this, impurity doping combined with the superior thermal conductivity and mechanical strength of AINNTs materials, improves significantly the sensing ability through the fusion of two different materials. What is interesting is, doped AlNNTs possess effective sensing ability and stability, which improves prospective sensing materials characteristics to detection and sensing. As a consequence, the search for new morphological adjustment of AlNNTs to improve sensing abilities is crucial for efficient device applications.

We employ density functional methodology to evaluate the effectiveness of both pristine AlNNT and Si-doped AlNNT (7,0) in detecting CO and CO_2 gases from atomistic point of view. We summarize the work as follows: (I) introduction (II)computational methodology (III) results and discussion (IV)conclusion.

2. Computational methodology

Our simulations are based on the first-principles method in the framework of density functional theory by using the Hohenberg and Kohn [56,57] formalism to calculate the intricate exchange-correlation effects of the many-body electron-electron interactions by the local density approximation (Perdue and Zunger parameterization [58], while nuclear and core interactions are represented by the Vanderbilt ultrasoft pseudopotential (USSD)) [59] scheme and the projected augment wave (PAW) technique to numerically reduce the number of plane waves needed for the convergence. The wavefunction and valence electron density are expanded with plane waves, and the Kohn-Sham orbitals are solved from the self-consistent field (SCF) calculation using the Davidson method of iterative diagonalization in the framework of pseudopotential methods. Using a modified Broyden [60] description, the ionic charge density is updated during the SCF cycle. To get the same accuracy for all the calculations, a kinetic energy cut-off of 60 R y was chosen after test. Brillouin zone sampling was done at the **Γ**-point for structures with 5 x 3 x 5, and the k-point meshes using the Monkhorst Pack grid of the supercell. Structural optimizations were carried out by the Broyden-Fletcher-Goldfarb-Shanno (BFGS) [61] optimization algorithm. All structures were fully relaxed until no atom had Hellman-Feynman forces greater than 0.001 R y/Bohr, and Gaussian smearing with a degauss value of 0.015 eV used. The computations performed using Quantum Espresso package [62,63] and its corresponding pseudopotential dataset.

The construction of models for the design structures were facilitated using Nanotube Builder [64] and Avogadro [65]. The molecular geometries of the structures were optimized using DFT [66] off-the shelf Quantum Espresso [67] code was used.

$$E_{ads} = E_{adsorbate\_adsorbent} - (E_{adsorbate} + E_{adsorbent}) \quad (1)$$

$$E_{ads}^{BSSE} = E_{adsorbate\_adsorbent} - (E_{adsorbate} + E_{adsorbent}) - \delta_{BSSE} \quad (2)$$

In the given formula, E_{ads} [68] signifies the adsorption energy, $E_{adsorbate\_adsorbent}$ refers to the cluster energy, $E_{adsorbate}$ represents the ground state energy of the geometry-optimized adsorbate molecule. In contrast, $E_{adsorbent}$ represents the energy of the geometry-optimized adsorbent molecule under investigation. Additionally, the provided E_{ads}^{BSSE} value was adjusted to account for the basis set superposition error (BSSE). To rectify the estimated E_{ads} affected by BSSE, the counterpoise correction (CP) method was applied by incorporating the δ_{BSSE} term into the interaction energy equation [69].

The Recovery Time (τ) [70]is an important factor in sensor construction since it is affected by the strength of the contact, which influences the complexity of the adsorption process. A larger negative E_{ads} number indicates a longer recovery period and similarly suggest strong

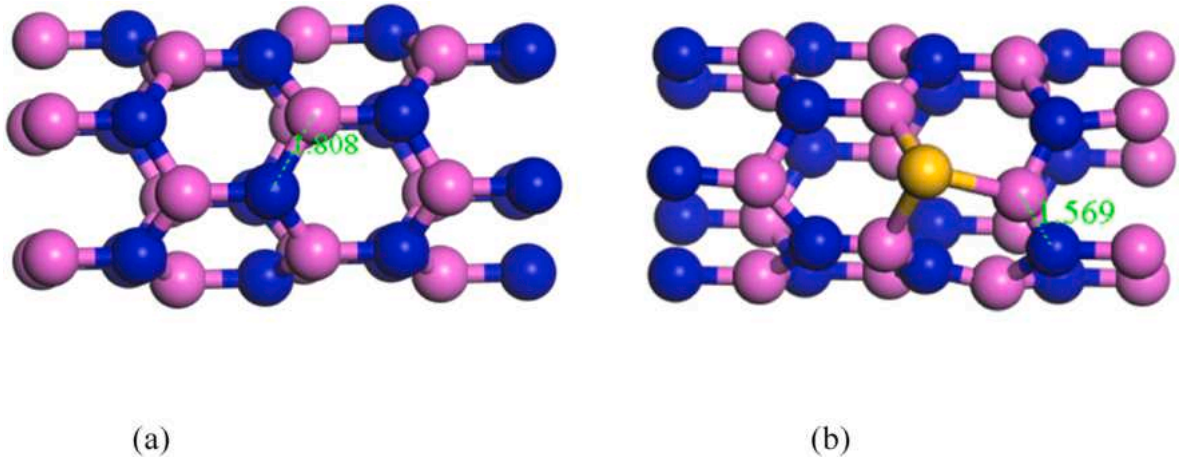

Fig. 1. Geometry optimized structure of (a) (7,0) AlNNT and (b) Si-(7,0) AlNNT with the bond length measured in Å

interaction [71].

$$\tau = vo^{-1} \exp\left(\frac{-E_{ads}}{kT}\right) \quad (3)$$

$$\tau^{BSSE} = vo^{-1} \exp\left(\frac{-E_{ads\ BSSE}}{kT}\right) \quad (4)$$

The variables are τ (recovery time), vo (frequency of attempts), k (Boltzmann's constant, about 2.0×10^{-3} kcal/mol. K), and T (temperature). Experiments show that different photonic frequencies (υ_0), thermal energy, and irradiation may be used to desorb molecules [72,73]. The experiment will use the parameters $\upsilon_0 = 10^{12}\ s^{-1}$ and T = 300 K for frequency and room temperature, respectively. The τ^{BSSE} is the recovery time after incorporating the BSSE correction factor. Equation (5) was used to compute the band gap (E_g) between the highest occupied molecular orbital (HOMO) and the lowest unoccupied molecular orbital (LUMO):

$$E_g = E_{LUMO} - E_{HOMO} \quad (5)$$

Here, the energy of the LUMO and the HOMO are represented by E_{LUMO} and E_{HOMO}, respectively. To evaluate the nanotube responsiveness, modifications to the energy gap (E_g) were calculated using the expression below:

$$\%\Delta E_g = \left[\left(E_{g2} - E_{g1}\right) / E_{g1}\right] \text{ x } 100 \quad (6)$$

Where ΔE_g represents the change in energy gap, E_{g1} signifies the energy gap of the AlNNTs, and E_{g2} denotes the energy gap of the AlNNTs-adsorbate complex.

Chemical potential (μ), global hardness (η), and electrophilicity index (ω) are pivotal for understanding the chemical reactivity and interaction stability. These descriptors aid in comprehending the energy equilibrium during charge transfers within a molecules chemical environment. The electrophilicity index (ω) exhibits a strong correlation with μ and η:

$$\omega = \mu^2/2\eta \quad (7)$$

The η parameter provides insights into the chemical system's resilience to changes in electron distribution. It is estimated as half of the energy difference between HOMO and LUMO. The chemical potential (μ) is calculated as the average of HOMO and LUMO energies.

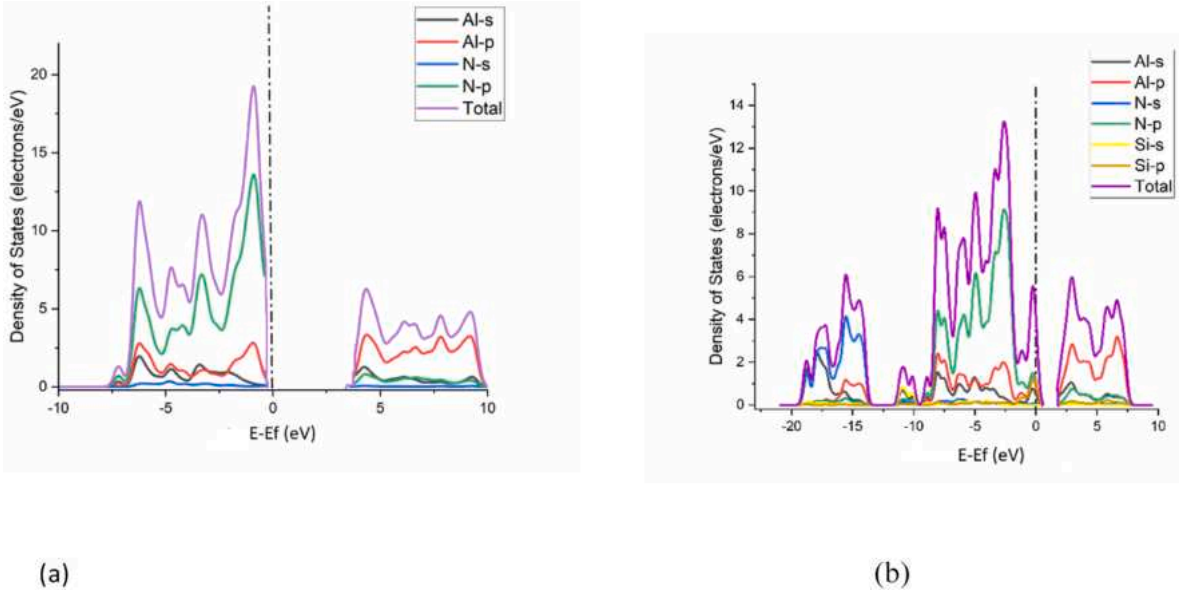

Fig. 2. The calculated density of state (DOS) and partial density of state (PDOS) for (a) (7,0) AlNNT and (b) Si-(7,0) AlNNT.

Table 1
The calculated adsorption energy (E_{ads}), calculated adsorption energy with the BSSE correction factor (E_{ads}^{BSSE}), HOMO and LUMO energies, band gap (E_g), chemical potential (μ), overall hardness (η), electrophilicity index (ω), recovery time (τ), recovery time with the BSSE correction factor (τ^{BSSE}) and sensing potential (% Δ Eg) for pristine, Si-doped and the nanotube/gases complexes are provided. E_{ads} is expressed in kcal/mol, τ in seconds, and other energy values are in electron volts (eV).

Model	E_{ads}	E_{ads}^{BSSE}	HOMO	LUMO	E_g	% Δ E_g	τ	τ^{BSSE}	μ	η	ω
(7,0) AlNNT	–	–	−6.243	−2.104	4.139	–	–	–	−4.174	2.070	4.208
Si-(7,0) AlNNT	–	–	−3.041	−3.387	1.846	–	–	–	−4.214	0.923	9.619
(7,0) AlNNT/CO_2	−23.58	−57.23	−6.239	−2.140	4.099	0.966	116,888.864	2.657×10^{40}	−4.190	2.050	4.282
Si-(7,0) AlNNT/CO_2	−17.56	−36.56	−3.181	−2.816	0.365	80.228	5.132	2.904×10^{25}	−3.000	0.183	24.590
(7,0) AlNNT/CO	−24.20	−44.32	−6.233	−2.152	4.081	1.401	328,506.603	1.202×10^{31}	−4.193	2.041	4.307
Si-(7,0) AlNNT/CO	−18.67	−40.54	−3.222	−2.861	0.361	80.444	32.643	2.207×10^{28}	−3.041	0.181	25.546

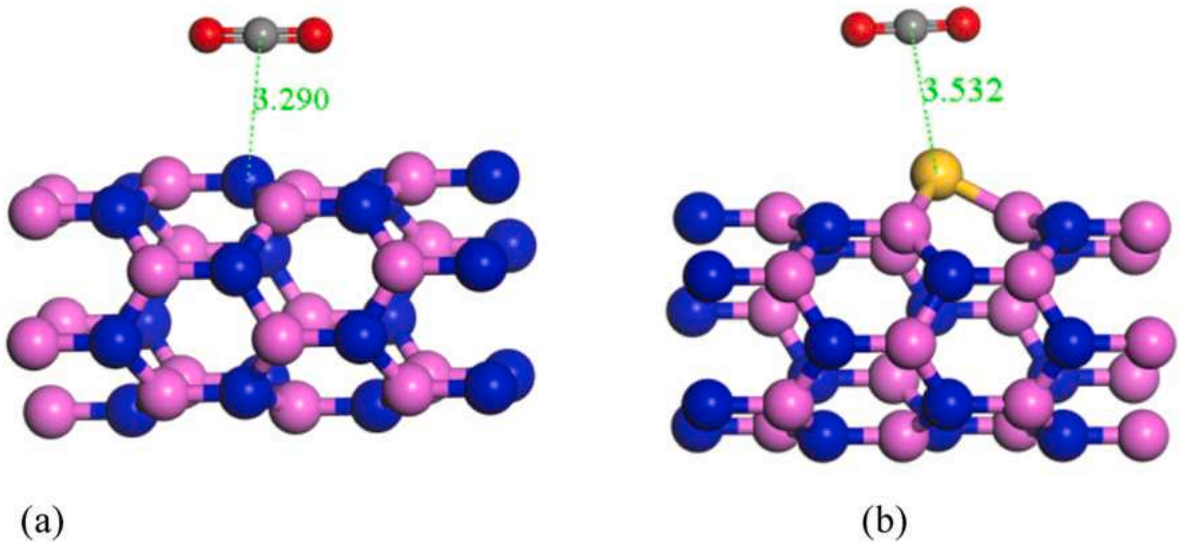

Fig. 3. Geometry optimized structure for (a) (7,0) AlNNT and (b) Si-(7,0) AlNNT interacting with CO_2, with the adsorption distance measured in Å.

3. Result and discussion

3.1. Pristine and Si-doped AlNNT properties

We have performed first principles calculations to examine the atomic and electronic structure of pristine (7,0)AlNNT and the corresponding Si-doped for the detection and adsorption of CO and CO_2 gases. The choice of (7,0) AlN nanotubes over other chiralities is primarily due to their favorable electronic properties, including being a direct band gap that enhances sensitivity to gas adsorption [74]. Additionally, the (7,0) configuration exhibits optimal stability and reactivity characteristics, making it particularly well-suited for effective sensing applications compared to other chiral forms [75].

For the calculations indicates that the atomic distance between Al and nitrogen N atoms in the (7,0) configuration is about 1.808 Å, as shown in Fig. 1(a). This value is consistent with the earlier findings by Mahdavifar [76], Abinya [75] groups, and us [77]. As a result of silicon doping shown in Fig. 1(b), the bond length between the Al and N significantly contracted to 1.569 Å. This reduction is a clear sign of the influence of the effect of silicon in the structure of the nanotube.

Additionally, from Fig. 2 and Table 1, the calculated pristine AlNNT's band gap (Eg) obtained from the difference between HOMO and LUMO as depicted by the partial density of states was found to be 4.14 eV, which indicates its wide bandgap semiconductor material. Following Si-doping, energy gap reduces to 1.85 eV. This reduction points to the emergence of new electronic states within the AlNNT originating mainly from the p-states of N and Al atoms and likely to modify the electrical and optical behaviour of the AlNNTs.

It is observed that, there is not much significant change in the chemical potential (μ) for both the pristine and Si-doped nanomaterials, suggesting that the Si dopant do not have any effect on the chemical potential of the composite system. Similarly, the global hardness (η) experiences a substantial drop of about 1.147 eV after doping between the pristine and the Si-doped AlNNT, implying that doped AlNNT may become more malleable to external forces. It was observed that after doping, electrophilicity index (ω) undergoes a significant increase of about 5.411 eV, suggesting a heightened inclination for the doped AlNNT to participate in chemical interactions.

In general, it was observed that, silicon doping has a significant impact on both the physical and chemical properties of AlNNT. The observed changes in bond length, band gap, chemical potential, global hardness, and electrophilicity index collectively indicate that silicon-doped AlNNT could altered electrical conductivity and a heightened reactivity, which may open up new applications for this material in various technological fields.

3.2. CO_2 adsorbed on (7,0) AlNNT and doped Si-(7,0) AlNNT

We analysed the adsorption of CO_2 onto aluminium nitride nanotubes with (7,0) chirality and corresponding Si-doped structure as shown in Fig. 3. The calculated adsorption energy for the pristine AlNNT and *Si*-AlNNT were ~-23.58 and ~-17.56 kal/mol respectively and their counter adsorption energies with BSSE correction factor were ~-57.23 and ~-36.56 kal/mol respectively. The chemisorption energies determined for the pristine structure was consistent with an earlier finding of Mahdavifar groups [78]. The adsorption energy measures the strength of the interacting complexes [79,80]. Therefore, the strong attractive force between the CO_2 molecule and the nanotube suggest strong interaction at the molecular level as can be inferred in Table 1 with adsorption energy difference of ~6 kal/mol between the pristine AlNNT and the corresponding Si doped. Perhaps this difference relates to the discernible alteration in the electronic properties between the two structures. As this

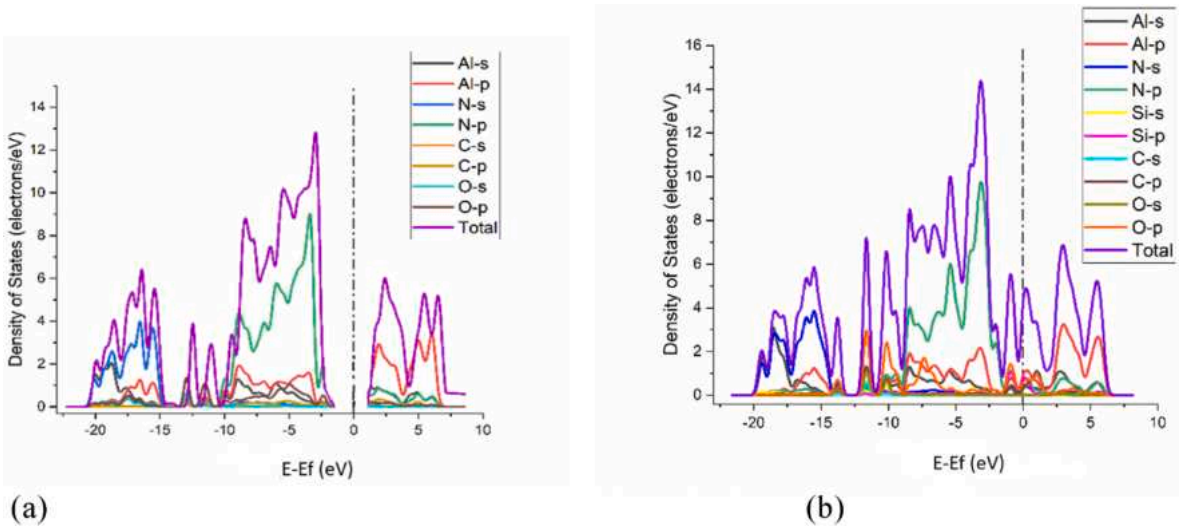

Fig. 4. The calculated density of state (DOS) and partial density of state (PDOS) for (a) (7,0) AlNNT and (b) Si-(7,0) AlNNT adsorbed with CO_2.

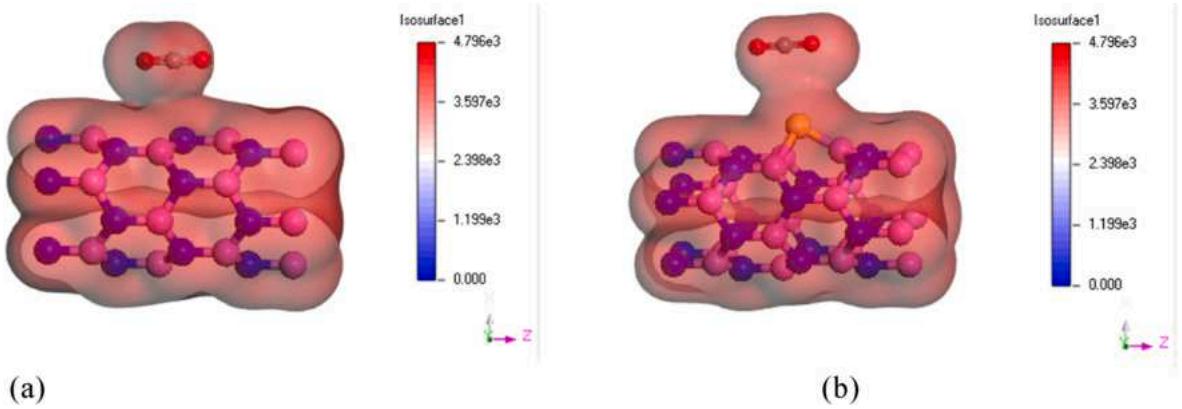

Fig. 5. The calculated valence charge density distribution for (a) (7,0) AlNNT and (b) Si-(7,0) AlNNT interacting with CO_2. The density is represented by the isovalue surface of 25 % of the maximum value.

is demonstrated by the modifications in the electronic levels of the HOMO and LUMO between them leading to a minor decrease in the bandgap of about 0.04 eV. However, there was relatively significant difference of about 3.734 eV between the AlNNT/CO_2 and *Si*-AlNNT/CO_2. Therefore, the reduced bandgaps between the doped and pristine AlNNTs with CO_2 suggest a potential increase in electrical conductivity post-adsorption.

These changes reflect the effect of CO_2 adsorptions on the electronic properties of the nanotubes due to the Si dopant. The calculated partial density of state (PDOS) and total density of state (DOS) as shown in Fig. 4 suggest major contribution from N-p state and moderate states from Al-p, Al-s and O-p at the Fermi level for CO_2 adsorption on the

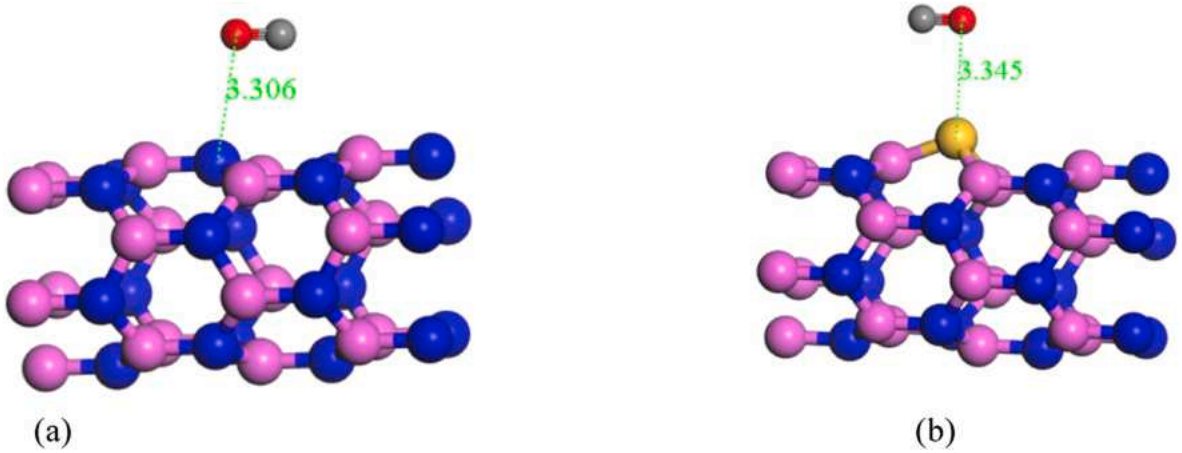

Fig. 6. Geometry optimized structure for (a) (7,0) AlNNT and (b) Si-(7,0) AlNNT interacting with CO, with the adsorption distance measured in Å.

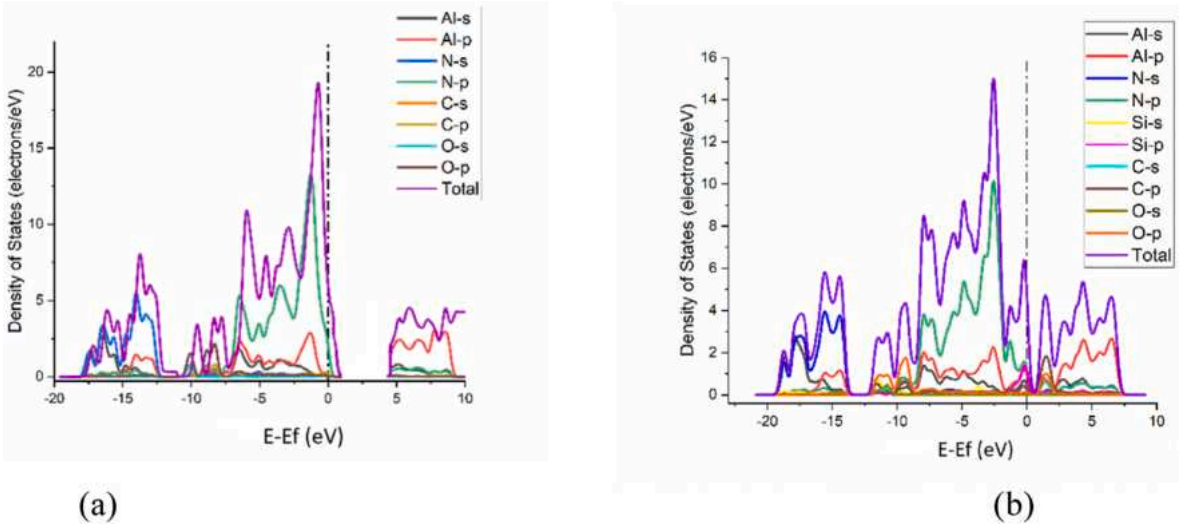

Fig. 7. The calculated density of state (DOS) and partial density of state (PDOS) for (a) (7,0) AlNNT and (b) Si-(7,0) AlNNT adsorbed with CO.

AlNNTs. However, with the Si-doped AlNNTs adsorption of CO_2, show strong hybridization exists between *Si*-p, O-p and Al-p with near disappearance of N-p state.

In spite of the strong interaction between *Si*-AlNNT and CO_2, the sensing potential was evaluated to be paltry 0.97 %, as shown in Table 1. This low potential value, coupled with slow recovery time of approximately 116,888 s (~1.35 days) may hinder the nanomaterial for practical usage as a CO_2 sensor for device application. However, the Si-doped AlNNT has a sensing potential estimated to be about 80.23 % for CO_2 suggesting a viable nanomaterial for the detection of CO_2 at the nano scale with impressive recovery time of just about ~5 s underscoring its suitability for rapid sensing devices.

When applying the basis set superposition error (BSSE) correction factor, the counter adsorption energies for the pristine AlNNT and *Si*-AlNNT were approximately −57.23 kcal/mol and −36.56 kcal/mol, respectively. However, the recovery times for the pristine AlNNT and Si-doped AlNNT increased significantly to approximately 2.657×10^{40} and 2.904×10^{25} s.

The study also shows that, the chemical potential, global hardness and eletrophilicity index for the *Si*-AlNNT shows propensity to participate in chemical reactions than the pristine AlNNT following adsorption of the CO_2 gas and similar properties could be observed with CO gas adsorption. The valence charge density distribution, in Fig. 5(a) and (b) shows the bonding between the CO_2 molecules and the nanotubes with significant charge transfer confirming the occurrence of these interactions, and responsible for the strong adsorption energies observed.

3.3. CO adsorbed on (7,0) AlNNT and Si-(7,0) AlNNT

We similarly examined the adsorption of CO onto chiral AlNNT (7,0) and corresponding Si-doped structures as indicated in Fig. 6 with calculated adsorption energy of ~ -24.20 and ~-18.67 kcal/mol for pristine AlNNT and *Si*-AlNNT structures respectively and their adsorption energies of ~ -44.32 and ~-40.54 kcal/mol when the BSSE correction factor is used. The calculated chemisorption energies were in agreement with Beheshtian [81] reported calculations.

The interactions between CO and nanotubes significantly modified the electronic characteristics of the nanomaterials under consideration.

The data presented in Table 1 from the recent study illustrates a substantial interaction between CO and the nanotubes. The strength of the interacting complexes depends on the adsorption energy at the molecular level. The difference in adsorption energy between the

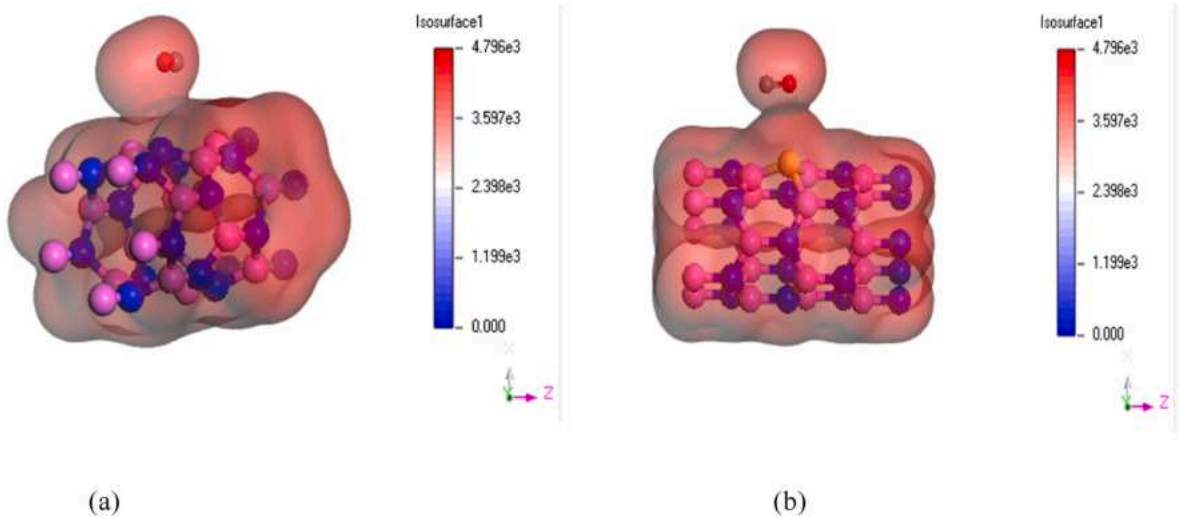

Fig. 8. The calculated valence charge density distribution for (a) (7,0) AlNNT and (b) Si-(7,0) AlNNT interacting with CO. The density is represented by the isovalue surface of 25 % of the maximum value.

pristine and the doped is about ~5.5 kal/mol and this might relate to the relative changes in their electronic properties of the two structures.

When the basis set superposition error (BSSE) correction factor was applied, the counter adsorption energies for the pristine AlNNT and *Si*-AlNNT were roughly −44.32 kcal/mol and −40.54 kcal/mol, respectively. In contrast, the recovery times for both the pristine AlNNT and Si-doped AlNNT increased dramatically, reaching approximately 1.202×10^{31} s and 2.207×10^{28} s.

The HOMO and LUMO energy difference which is the bandgap energy did not show any appreciable variation between the pristine and the AlNNT/CO composite which is about 0.058 eV. However, the bandgap energy difference between the AlNNT/CO and the *Si*-AlNNT/CO complexes is about 3.72 eV when compared. This clearly reflects the observed changes in the electronic properties of the nanotubes upon CO adsorption as consequence of the Si doping which clearly improves the electrical conductivity after the adsorption. This observation is similar when CO_2 gas was adsorbed. The calculated PDOS and DOS for AlNNT/CO and *Si*-AlNNT/CO structures are shown in Fig. 7. It is observed that, the major contributing states in the hybridization process originates mainly from the N-p state. We find mixed Al-p and O-p states at the Fermi level with the pristine CO adsorption sites whilst moderate C-p and *Si*-p states with the Si-doped CO adsorption. This clearly reflects the electronic structure of the nanotubes upon CO adsorption bonding mechanism.

The Si-(7,0) AlNNT demonstrated a high sensing potential of about 80.44 %, with relatively short recovery time of about 32.64 s or (0.56 min) whereas pristine AlNNT showed a rather low sensing potential of 1.40 % and long recovery time of 328,506.0 s (3.80 days) of CO adsorption. These results further support the sensing potential for the Si-(7,0) AlNNT to be used in real-time CO sensing devices, as they can quickly reset after detecting CO. However, (7,0) AlNNT's sensor responsiveness needs enhancement for practical applications.

The chemical potential changes post-adsorption between the AlNNT/CO and *Si*-AlNNT/CO showed difference of 1.1 5 eV compared between the pristine AlNNT and the doped *Si*-AlNNT is marginal 0.02 eV, the former clearly show improve reactivity of the Si-doped nanomaterial. Similarly, global hardness change was observed to be about 1.86 eV with increase in the *Si*-AlNNT/CO doped compared with the AlNNT/CO. There was sharp in increase in the electrophilicity index of 21.24 eV towards *Si*-AlNNT/CO with respect to AlNNT/CO and about two-fold when with compared *Si*-AlNNT.

These results suggest an emergence of new chemical states within the nanotube structures due to the doping as illustrated in Fig. 7 (b) and also nanotubes become more malleable and less resistant to external forces after CO adsorptions. The valence charge densities illustration Fig. 8 demonstrates the development of combined states between the CO molecules and the surfaces of the nanotubes with strong bonding. These hybridizations are as a result of the interactions between the CO and AlNNT indicating a sharing or transfer of charges between them.

In general, we observed that the interactions of CO with the nanotubes have been shown to create a strong interacting bond which affects the electronic properties of the nanotubes. Though there is sensing potential for the pristine AlNNT, the long recovery time highlights the need for further development to improve the practicality of this nanotubes as sensor. However, the high sensing potential and short recovery time for CO on Si-(7,0) AlNNT out surface suggest Si-(7,0) AlNNT is a promising candidate for CO_2 sensing. The observed changes in chemical potential, global hardness, and electrophilicity index, along with the formation of a hybrid state, provide insights into the nature of the CO adsorption on (7,0) AlNNT and Si-(7,0) AlNNT.

4. Conclusion

In summary, the computational study delved into the mechanism of CO_2 and CO gases adsorption when in contact with pristine (7,0) and Silicon-doped (7,0) AlNNT. The investigation revealed that CO_2 adheres strongly to (7,0) AlNNT, which is indicative of its ability to function as a CO_2 detector. Nonetheless, the extended time it takes for the sensor to reset could be a drawback for real-world usage. The adsorption of CO_2 also alters the electronic structure of (7,0) AlNNT, leading to a reduced band gap and modifications to the HOMO and LUMO levels. In a similar way, CO adherence to (7,0) AlNNT was robust, pointing to its suitability as a CO detector, with considerable recovery time suggest the need for improvement. The bond between CO_2 and Si-doped (7,0) AlNNT was also strong, accompanied by a narrowing of the band gap and the emergence of novel electronic states. The Si-doped nanotubes demonstrated a strong potential for CO_2 detection, benefiting from a quick recovery time. Moreover, the interaction of CO with Si-(7,0) AlNNT was favorable, leading to significant adsorption and alterations in the chemical potential, global hardness, and electrophilicity index, suggesting its viability for CO detection. Analysis of charge density distributions provided a deeper understanding of the electronic interactions and charge transfers involved. In short, the study clarifies the potential use of both pristine and Si-doped aluminium nitride nanotubes use for CO_2 and CO detection and offers a comprehensive view of their electronic characteristics and their interactions.

CRediT authorship contribution statement

Nafiu Suleiman: Investigation, Formal analysis, Data curation. **Vitus Apalangya:** Investigation, Visualization, Methodology, Data curation. **Kwabena Kan-Dapaah:** Conceptualization, Writing – review & editing. **Bismark Mensah:** Formal analysis, Validation, Software, Writing – review & editing. **Van W. Elloh:** Methodology, Investigation, Formal analysis. **Abu Yaya:** Resources, Project administration, Funding acquisition. **Eric K.K. Abavare:** Writing – review & editing, Writing – original draft, Supervision, Project administration, Formal analysis.

Declaration of competing interest

The authors declare that they have no known competing financial interests or personal relationships that could have appeared to influence the work reported in this paper.

Acknowledgement

We have performed all calculations with the help of the South African Centre for High-Performance Computing (CHPC). Nafiu, acknowledges CHPC for the use of the computing resources.

Data availability

Data will be made available on request.

References

[1] E. Green, S. Short, L.K. Shuker, P.T.C. Harrison, Carbon monoxide exposure in the home environment and the evaluation of risks to health - a UK perspective, Indoor Built Environ. 8 (3) (1999) 168–175, https://doi.org/10.1159/000024632.
[2] H. Kinoshita, et al., Carbon monoxide poisoning, Toxicol Rep 7 (October 2019) 169–173, https://doi.org/10.1016/j.toxrep.2020.01.005, 2020.
[3] E. Picano, C. Mangia, A. D'Andrea, Climate change, carbon dioxide emissions, and Medical Imaging contribution, J. Clin. Med. 12 (1) (2023) 1–9, https://doi.org/10.3390/jcm12010215.
[4] R. Kawamoto, et al., Estimation of CO2 Emissions of internal combustion engine vehicle and battery electric vehicle using LCA, Sustainability 11 (9) (2019), https://doi.org/10.3390/su11092690.
[5] P. Bierwirth, Long-term Carbon Dioxide Toxicity and Climate Change : a Major Unapprehended Risk for Human Health Long-Term Carbon Dioxide Toxicity and Climate Change : a Major Unapprehended Risk for Human Health, October, 2022, https://doi.org/10.13140/RG.2.2.16787.48168.
[6] N. Johansen, Carbon Monoxide Detection and Alarm Requirements : Literature Review Final Report by, February, 2021.
[7] M. v Hnatov, "Non-Fire Carbon Monoxide Deaths Associated with the Use of Consumer Products: 2007 Annual Estimates, January 2011," no. December, 2011.

[8] P.W. Francisco, S. Pigg, D. Cautley, W.B. Rose, D.E. Jacobs, S. Cali, Carbon monoxide measurements in homes, Sci Technol Built Environ 24 (2) (2018) 118–123, https://doi.org/10.1080/23744731.2017.1372806.

[9] D.S. Fisher, S. Bowskill, L. Saliba, R.J. Flanagan, Unintentional domestic non-fire related carbon monoxide poisoning: data from media reports, UK/Republic of Ireland 1986-2011, Clin. Toxicol. 51 (5) (2013) 409–416, https://doi.org/10.3109/15563650.2013.786833.

[10] J. Long, Y. Sun, J. Zhao, J. Liu, X. Peng, Temporal trends of carbon monoxide poisoning mortality at the global, regional and national levels: a cross-sectional study from the Global Burden of Disease study, 1990 and 2017, BMJ Open 11 (11) (2021), https://doi.org/10.1136/bmjopen-2021-053240.

[11] A.I. Al-Asmari, A.E. Al-Zahrani, M.A. Halwani, Carbon monoxide related deaths in Jeddah, Saudi Arabia: a forensic carboxyhemoglobin autopsy-based study, Forensic Sci. Int.: Report 4 (2021) 100232, https://doi.org/10.1016/j.fsir.2021.100232.

[12] M.W. Saleem, M.H. Tahir, M.W. Ashfaq, Fossil Fuel Based Carbon Footprint of Pakistan and its Role towards Fossil Fuel Based Carbon Footprint of Pakistan and its Role towards Sustainable Development, 2020. February.

[13] M. Zimakowska-Laskowska, P. Laskowski, Emission from internal combustion Engines and battery electric vehicles: Case study for Poland, Atmosphere 13 (3) (2022) 1–8, https://doi.org/10.3390/atmos13030401.

[14] W.F. Lamb, et al., A review of trends and drivers of greenhouse gas emissions by sector from 1990 to 2018, Environ. Res. Lett. 16 (7) (2021) 73005, https://doi.org/10.1088/1748-9326/abee4e.

[15] X.L. Yue, Q.X. Gao, Contributions of natural systems and human activity to greenhouse gas emissions, Adv. Clim. Change Res. 9 (4) (2018) 243–252, https://doi.org/10.1016/j.accre.2018.12.003.

[16] G. Marland, R.M. Rotty, Carbon dioxide emissions from fossil fuels: a procedure for estimation and results for 1950-1982, Tellus 36 D (4) (1984) 232–261, https://doi.org/10.3402/tellusb.v36i4.14907.

[17] D. Kweku, et al., Greenhouse effect: greenhouse gases and their impact on global warming, J Sci Res Rep 17 (6) (2018) 1–9, https://doi.org/10.9734/jsrr/2017/39630.

[18] R.T. Venterea, Climate change 2007: Mitigation of climate change, J. Environ. Qual. 38 (2) (2009), https://doi.org/10.2134/jeq2008.0024br, 837–837.

[19] G.A. Florides, P. Christodoulides, Global warming and carbon dioxide through sciences, Environ. Int. 35 (2) (2009) 390–401, https://doi.org/10.1016/j.envint.2008.07.007.

[20] J. Ahn, et al., Atmospheric CO2 over the last 1000 years: a high-resolution record from the west Antarctic Ice Sheet (WAIS) Divide ice core, Global Biogeochem. Cycles 26 (2) (2012), https://doi.org/10.1029/2011GB004247.

[21] C. le Quéré, et al., Trends in the sources and sinks of carbon dioxide, Nat. Geosci. 2 (12) (2009) 831–836, https://doi.org/10.1038/ngeo689.

[22] M.A. El-Sharkawy, Global warming: causes and impacts on agroecosystems productivity and food security with emphasis on cassava comparative advantage in the tropics/subtropics, Photosynthetica 52 (2) (2014) 161–178, https://doi.org/10.1007/s11099-014-0028-7.

[23] A. Carolina Sparavigna, Carbon dioxide concentration and emissions in Atmosphere: trends and Recurrence Plots, Intermt. J. Sci. 0 (10) (2014) 8–15, https://doi.org/10.18483/ijsci.582.

[24] K.E. Trenberth, et al., Global warming and changes in drought, Nat. Clim. Change 4 (1) (2014) 17–22, https://doi.org/10.1038/nclimate2067.

[25] J.-P. Vidal, J.-M. Soubeyroux, Impact of climate change on drought and soil moisture in France, in: SEC2008 - International Symposium - Drought and Constructions, 2008, pp. 25–31. July.

[26] G.R. North, Global climate change, in: A World after Climate Change and Culture-Shift, 2014, pp. 25–42, https://doi.org/10.1007/978-94-007-7353-0_3. April.

[27] W. Marx, R. Haunschild, L. Bornmann, Heat waves: a hot topic in climate change research, Theor. Appl. Climatol. 146 (1–2) (2021) 781–800, https://doi.org/10.1007/s00704-021-03758-y.

[28] Z.W. Kundzewicz, Extreme weather events and their consequences, Papers on Global Change IGBP 23 (1) (2016) 59–69, https://doi.org/10.1515/igbp-2016-0005.

[29] K.L. Ebi, et al., Extreme weather and climate change: Population health and health system Implications, Annu. Rev. Publ. Health 42 (2020) 293–315, https://doi.org/10.1146/annurev-publhealth-012420-105026.

[30] S. Mukherjee, A. Mishra, K.E. Trenberth, Climate change and drought: a perspective on drought Indices, Curr. Clim. Change Rep. 4 (2) (2018) 145–163, https://doi.org/10.1007/s40641-018-0098-x.

[31] D.S. Matawal, D.J. Maton, Climate change and global warming: signs, impact and solutions, Int. J. Environ. Sustain Dev. (January) (2013) 62–66, https://doi.org/10.7763/ijesd.2013.v4.305.

[32] P. Martinez, E.R. Bandala, Heat Waves : A Growing Climate Change-Related Risk, 2016, pp. 1–3. February.

[33] Y. Xia, D. Guan, X. Jiang, L. Peng, H. Schroeder, Q. Zhang, Assessment of socioeconomic costs to China's air pollution, Atmos. Environ. 139 (2016) 147–156, https://doi.org/10.1016/j.atmosenv.2016.05.036.

[34] J.C. Ciscar, et al., Physical and economic consequences of climate change in Europe, Proc Natl Acad Sci U S A 108 (7) (2011) 2678–2683, https://doi.org/10.1073/pnas.1011612108.

[35] X. Xu, H. Yang, C. Li, Theoretical model and actual characteristics of air pollution affecting health cost: a review, Int. J. Environ. Res. Publ. Health 19 (6) (2022), https://doi.org/10.3390/ijerph19063532.

[36] S.S. Saurabh Sonwani, V.M. Vandana Maurya, Impact of air pollution on the environment and economy, Air pollution: sources, impacts and controls (2019) 113–134, https://doi.org/10.1079/9781786393890.0113. December 2018.

[37] C. Meisner, D. Gjorgjev, F. Tozija, Estimating health impacts and economic costs of air pollution in the Republic of Macedonia, South East Eur J Public Health 10 (April) (2015) 1–8, https://doi.org/10.12908/SEEJPH-2014-45.

[38] J. Szlávik, M. Füle, Economic consequences of climate change, AIP Conf. Proc. 1157 (2009) 73–82, https://doi.org/10.1063/1.3208034.

[39] M. Noei, H. Soleymanabadi, A.A. Peyghan, Aluminum nitride nanotubes, Chem. Pap. 71 (5) (2017) 881–893, https://doi.org/10.1007/s11696-016-0015-5.

[40] S. Hao, L. Zhang, X. Wang, G. Zhao, P. Hou, X. Xu, Design of multilayered porous aluminum nitride for supercapacitor applications, Energy Fuel. 35 (15) (2021) 12628–12636, https://doi.org/10.1021/acs.energyfuels.1c01420.

[41] J. Beheshtian, M.T. Baei, Z. Bagheri, A.A. Peyghan, AlN nanotube as a potential electronic sensor for nitrogen dioxide, Microelectron. J. 43 (7) (2012) 452–455, https://doi.org/10.1016/j.mejo.2012.04.002.

[42] N. Zheng, C. Zhang, R. Fan, Z. Sun, Melamine foam-based shape-stable phase change composites enhanced by aluminum nitride for thermal management of lithium-ion batteries, J. Energy Storage 52 (PC) (2022) 105052, https://doi.org/10.1016/j.est.2022.105052.

[43] Q. Wu, et al., Synthesis and characterization of faceted hexagonal aluminum nitride nanotubes, J. Am. Chem. Soc. 125 (34) (2003) 10176–10177, https://doi.org/10.1021/ja0359963.

[44] L.W. Yin, Y. Bando, Y.C. Zhu, M. sen Li, C.C. Tang, D. Golberg, Single-crystalline AlN nanotubes with carbon-layer coatings on the outer and inner surfaces via a multiwalled-carbon-nanotube-template-induced route, Adv. Mater. 17 (2) (2005) 213–217, https://doi.org/10.1002/adma.200400105.

[45] M. Hesabi, M. Hesabi, The interaction between carbon nanotube and skin anti-cancer drugs: a DFT and NBO approach, J Nanostructure Chem 3 (1) (2013) 1–6, https://doi.org/10.1186/2193-8865-3-22.

[46] A. Ahmadi Peyghan, A. Omidvar, N.L. Hadipour, Z. Bagheri, M. Kamfiroozi, Can aluminum nitride nanotubes detect the toxic NH 3 molecules? Physica E Low Dimens Syst Nanostruct 44 (7–8) (Apr. 2012) 1357–1360, https://doi.org/10.1016/j.physe.2012.02.018.

[47] A.V. Kuzmin, B.A. Shainyan, Single Si-doped graphene as a catalyst in oxygen reduction reactions: an in silico study, ACS Omega 5 (25) (2020) 15268–15279, https://doi.org/10.1021/acsomega.0c01303.

[48] J. xiang Zhao, Y. Chen, H. gang Fu, Si-embedded graphene: an efficient and metal-free catalyst for CO oxidation by N2O or O2, Theor. Chem. Acc. 131 (6) (2012) 1–11, https://doi.org/10.1007/s00214-012-1242-7.

[49] M. Ghanbari, S. Afshari, S.A. Nabavi Amri, New capability of graphene as hydrogen storage by Si and/or Ge doping: density functional theory, Int. J. Hydrogen Energy 45 (43) (2020) 23048–23055, https://doi.org/10.1016/j.ijhydene.2020.06.039.

[50] M. Shahabi, H. Raissi, Investigation of the molecular structure, electronic properties, AIM, NBO, NMR and NQR parameters for the interaction of Sc, Ga and Mg-doped (6,0) aluminum nitride nanotubes with COCl2 gas by DFT study, J. Inclusion Phenom. Macrocycl. Chem. 84 (1–2) (2015) 99–114, https://doi.org/10.1007/s10847-015-0587-7.

[51] A. Ahmadi, N.L. Hadipour, M. Kamfiroozi, Z. Bagheri, Theoretical study of aluminum nitride nanotubes for chemical sensing of formaldehyde, Sens Actuators B Chem 161 (1) (2012) 1025–1029, https://doi.org/10.1016/j.snb.2011.12.001.

[52] Z. Mahdavifar, N. Abbasi, The influence of Cu-doping on aluminum nitride, silicon carbide and boron nitride nanotubes' ability to detect carbon dioxide; DFT study, Physica E Low Dimens Syst Nanostruct 56 (2014) 268–276, https://doi.org/10.1016/j.physe.2013.09.008.

[53] M. Mirzaei, A. Seif, N.L. Hadipour, The C-doped zigzag AlN nanotube: a computational NMR study, Chem. Phys. Lett. 461 (4–6) (2008) 246–248, https://doi.org/10.1016/j.cplett.2008.07.024.

[54] A. Soltani, S.G. Raz, V.J. Rezaei, A. Dehno Khalaji, M. Savar, Ab initio investigation of Al- and Ga-doped single-walled boron nitride nanotubes as ammonia sensor, Appl. Surf. Sci. 263 (2012) 619–625, https://doi.org/10.1016/j.apsusc.2012.09.122.

[55] Y. Cao, M. Farahmand, R. Ahmadi, M. Reza Poor Heravi, S. Ahmadi, M. Z. Mahmoud, Unraveling the effect of Ti doping on the sensing properties of AlN nanotubes toward acrylonitrile gas, Inorg. Chem. Commun. 137 (December 2021) (2022) 109161, https://doi.org/10.1016/j.inoche.2021.109161.

[56] P. Hohenberg, W. Kohn, Inhomogeneous electron gas, Phys. Rev. 136 (1964) B1864, https://doi.org/10.1103/PhysRev.136.B864.

[57] W. Kohn, L.J. Sham, Self-consistent equations including exchange and correlation effects, Phys. Rev. 385 (1951) (1965), https://doi.org/10.1103/PhysRev.140.A1133.

[58] J.P. Perdew, A. Zunger, Self-interaction correction to density-functional approximations for many-electron systems, Phys. Rev. B 23 (10) (1981) 5048–5079, https://doi.org/10.1103/PhysRevB.23.5048.

[59] D. Vanderbilt, Rapid Communications 41 (11) (1990) 7892–7895.

[60] D.D. Johnson, " Modified Broyden's method for accelerating convergence in self-consistent calculations", Phys. Rev. B 38 (18) (1988) 12807–12813.

[61] J.D. Head, M.C. Zerner, A Broyden-Fletcher-Goldfarb-Shanno optimization procedure for molecular geometries, Chem. Phys. Lett. 122 (3) (1985) 264–270, https://doi.org/10.1016/0009-2614(85)80574-1.

[62] P. Giannozzi, et al., Q uantum espresso : a modular and open-source software project for quantum simulations of materials 395502 (2009), https://doi.org/10.1088/0953-8984/21/39/395502.

[63] P. Giannozzi, et al., Advanced capabilities for materials modelling with Quantum ESPRESSO, J. Phys. Condens. Matter 29 (46) (2017), https://doi.org/10.1088/1361-648X/aa8f79.

[64] N.A. Sakharova, J.M. Antunes, A.F.G. Pereira, J.v. Fernandes, Developments in the evaluation of elastic properties of carbon nanotubes and their heterojunctions by

numerical simulation, AIMS Mater Sci 4 (3) (2017) 706–737, https://doi.org/10.3934/matersci.2017.3.706.
[65] B. Rayan, A. Rayan, Avogadro program for chemistry education: to what extent can molecular visualization and three-dimensional simulations enhance meaningful chemistry learning? World Journal of Chemical Education 5 (4) (2017) 136–141, https://doi.org/10.12691/wjce-5-4-4.
[66] K.M. Batoo, I.S. Alalaq, M.M. Rkha, A. Mishra, S. Sharma, G.V. Siva Prasad, M. F. Ijaz, S.B. Alsaadi, A.A. Mtasher, F.F. Seed, A novel MoS2/Pd5 nanocluster heterojunction system with improved surface reactivity for efficient gas sensing: a DFT study, Surf. Sci. 752 (2024), https://doi.org/10.1016/j.susc.2024.122648 (Feb).
[67] S. Nafiu, V.A. Apalangya, A. Yaya, E.B. Sabi, Boron nitride nanotubes for curcumin delivery as an anticancer drug: a DFT investigation, Appl. Sci. 12 (2) (2022), https://doi.org/10.3390/app12020879.
[68] M.D. Ganji, M. Rezvani, Boron nitride nanotube based nanosensor for acetone adsorption: a DFT simulation, J. Mol. Model. 19 (3) (Mar. 2013) 1259–1265, https://doi.org/10.1007/s00894-012-1668-9.
[69] A. Rahmanzadeh, M. Rezvani, M. Darvish Ganji, M. Tale Moghim, Corrosion protection performance of Laurhydrazide N′-propan-3-one (LHP) adsorbed on zinc surface: a DFT-MD simulation investigation, Mater. Today Commun. 36 (Aug) (2023), https://doi.org/10.1016/j.mtcomm.2023.106946.
[70] M.D. Ganji, S. Jameh-Bozorgi, M. Rezvani, A comparative study of structural and electronic properties of formaldehyde molecule on monolayer honeycomb structures based on vdW-DF prospective, Appl. Surf. Sci. 384 (Oct. 2016) 175–181, https://doi.org/10.1016/j.apsusc.2016.05.011.
[71] T. Banibairami, S. Jamehbozorgi, R. Ghiasi, M. Rezvani, Sensing Behavior of Hexagonal-Aluminum Nitride to Phosgene Molecule Based on Van der Waals–Density Functional Theory and Molecular Dynamic Simulation, Russ. J. Phys. Chem. A 94 (3) (Mar. 2020) 581–589, https://doi.org/10.1134/S0036024420030048.
[72] A.A. Menazea, N.S. Awwad, H.A. Ibrahium, G. Ebaid, H. Elhosiny Ali, Selective detection of sulfur trioxide in the presence of environmental gases by AlN nanotube, J. Sulfur Chem. 43 (3) (2022) 290–303, https://doi.org/10.1080/17415993.2021.2016764.
[73] Y. Wang, B. Liu, R. Fang, L. Jing, P. Wu, S. Tian, Adsorption and Sensing of CO_2, CH_4 and N_2O Molecules by Ti-Doped HfSe 2 Monolayer Based on the First-Principle, 2022, pp. 1–12, cc.
[74] M. Zhao, Y. Xia, D. Zhang, L. Mei, Stability and electronic structure of AlN nanotubes, Phys. Rev. B Condens. Matter 68 (23) (Dec. 2003), https://doi.org/10.1103/PhysRevB.68.235415.
[75] V. Abinaya, D. John Thiruvadigal, R. Akash, A. Sakthi Balaji, R.M. Hariharan, J. Sneha, U. Adharsh, K. Janani Sivasankar, "Chemical modification of aluminum nitride nanotubes (AlNNT) using-OH, C=O, R-SH functional groups: first principle's study, Surface. Interfac. 41 (2023) 103–262, https://doi.org/10.1016/j.surfin.2023.103262. ISSN 2468-0230.
[76] Z. Mahdavifar, M. Haghbyan, M. Abbasi, Theoretical investigation of ethane and ethene monitoring using pristine and decorated aluminium nitride and silicon carbide nanotubes, Sensors Actuators, B Chem. 196 (2014) 555–566, https://doi.org/10.1016/j.snb.2014.02.048.
[77] N. Suleiman, V.A. Apalangya, B. Mensah, K. Kan-Dapaah, A. Yaya, Exploring carbon monoxide and carbon dioxide adsorption on (5,5) aluminum nitride nanotubes for enhanced sensor applications: a DFT study, Molecules 29 (3) (2024), https://doi.org/10.3390/molecules29030557.
[78] Z. Mahdavifar, N. Abbasi, E. Shakerzadeh, A comparative theoretical study of CO_2 sensing using inorganic AlN, BN and SiC single walled nanotubes, Sens Actuators B Chem 185 (2013) 512–522, https://doi.org/10.1016/j.snb.2013.05.004.
[79] M.D. Ganji, Theoretical study of the adsorption of CO2 on tungsten carbide nanotubes, Physics Letters, Section A: General, Atomic and Solid State Physics 372 (18) (Apr. 2008) 3277–3282, https://doi.org/10.1016/j.physleta.2008.01.032.
[80] J. Beheshtian, Z. Bagheri, M. Kamfiroozi, A. Ahmadi, A theoretical study of CO adsorption on aluminum nitride nanotubes, Struct. Chem. 23 (2012) 653–657. https://api.semanticscholar.org/CorpusID:96240574.
[81] J.S. Gaffney, N.A. Marley, The impacts of combustion emissions on air quality and climate - from coal to biofuels and beyond, Atmos. Environ. 43 (1) (2009) 23–36, https://doi.org/10.1016/j.atmosenv.2008.09.016.